Numerical simulations of strongly correlated fermions confined in 1D optical lattices

Marcos Rigol and Alejandro Muramatsu

Institut für Theoretische Physik III, Universität Stuttgart, Pfaffenwaldring 57, D-70550 Stuttgart, Germany.

Abstract

On the basis of quantum Monte Carlo (QMC) simulations we study the formation of Mott domains in the one-dimensional Hubbard model with an additional confining potential. We find evidences of quantum critical behavior at the boundaries of the Mott-insulating regions. A local compressibility defined to characterize the local phases exhibits a non-trivial critical exponent on entering the Mott-insulating domains. Both the local compressibility and the variance of the local density show universality with respect to the confining potential. We also study the momentum distribution function of the trapped system, and determine its phase diagram.

Key words: Optical lattices, metal–Mott-insulator transition, Degenerated Fermi gases, Strongly correlated systems
PACS: 03.75.Ss, 05.30.Fk, 71.30.+h

1 Introduction

The study of ultracold quantum gases has become in the last decade a field of intense experimental and theoretical research [1,2,3,4]. Bose-Einstein condensation (BEC) was the main motivation starting the intensive analysis of such systems. It was observed for the first time in a series of experiments on dilute vapors of alkali atoms cooled down to extremely low temperatures (fractions of microkelvins) [5,6,7].

Recently, new features that allow to go beyond the weakly interacting regime and access strongly correlated limits have been added to the experiments. Particularly important, due to its relevance for condensed matter physics, has been the introduction of optical lattices. They allowed the study of the superfluid–Mott-insulator phase transition in three-dimensional [8], and one-dimensional (1D) [9] systems. The presence of the optical lattice and the fact that the particles interact only via contact interaction, lead in a natural way

to the Hubbard model as a paradigm for these systems. A theoretical work proposing such experiments [10], and quantum Monte Carlo (QMC) simulations [11,12,13] have examined these systems in detail. It has been found that incompressible Mott insulating phases appear for wide ranges of fillings, and always coexist with compressible phases, so that local order parameters [11,13] have to be defined to characterize the system.

In the fermionic case, the metal–Mott-insulator transition (MMIT) [14,15] has not been observed yet. However, recent experiments succeeded in loading single species ultracold fermionic gases on an optical lattice [16,17], allowing the realization of an ideal Fermi gas on a lattice. Progress in this field, loading more than one component fermions and reducing the occupation per lattice site, could lead to the realization of the metal–Mott-insulator transition on optical lattices.

Motivated by this expectation we studied, using QMC simulations, the ground state of the one dimensional (1D) fermionic Hubbard model with a harmonic trap [14,15]. In the present work we review those references adding some new results and improving others. As in the bosonic case [11,12,13], we find that Mott domains appear over a continuous range of fillings and always coexist with compressible phases. Therefore, we define a local order parameter, that we call local compressibility, in order to characterize the local phases present in the system. By means of this local compressibility, we analyze in detail the interface between the metallic and insulating region finding that critical behavior sets in, revealing a new critical exponent. Furthermore, the behavior of the local compressibility and the variance of the density are found to be universal in this case independently of the confining potential and the strength of the interaction. Hence, universality appears as usual in critical phenomena. The momentum distribution function, a quantity usually accessed in the experiments, is studied in detail. The results obtained show that due to the inhomogeneous character of these systems, this quantity does not exhibit a clear signature of the formation of Mott domains. Finally, we obtain the phase diagram for fermions confined in 1D harmonic traps. It allows to compare systems with different fillings and curvatures of the confining potential, so that it could help to understand future experimental results.

The exposition is organized as follows. In the next section, we give a short introduction to the Hubbard model on periodic systems. In Sec. 3, we study local quantities within the Hubbard model with an additional harmonic trap. In particular, we define a local compressibility that acts as a local order parameter to characterize the Mott-insulating phases. In Sec. 4, we study in detail the region where the transition between the metallic and the Mott-insulating phases occurs. The momentum distribution function is analyzed in Sec. 5. In Sec. 6, we discuss the phase diagram for these systems. Finally, the conclusions are given in Sec. 7.

2 The Hubbard model

The Hubbard model in a periodic lattice [18,19] has been intensively studied in condensed matter physics as a prototype for the theoretical understanding of the MMIT. This model considers electrons in a single band, and its Hamiltonian can be written as

$$H = -t \sum_{i,\sigma} \left(c_{i\sigma}^\dagger c_{i+1\sigma} + \text{H.c.} \right) + U \sum_i n_{i\uparrow} n_{i\downarrow} \tag{1}$$

where $c_{i\sigma}^\dagger$, $c_{i\sigma}$ are creation and annihilation operators, respectively, for electrons with spin σ at site i, and $n_{i\sigma} = c_{i\sigma}^\dagger c_{i\sigma}$ is the particle number operator. Electrons are considered to hop only between nearest neighbors with a hopping amplitude t, and the on-site interaction parameter is denoted by U ($U > 0$).
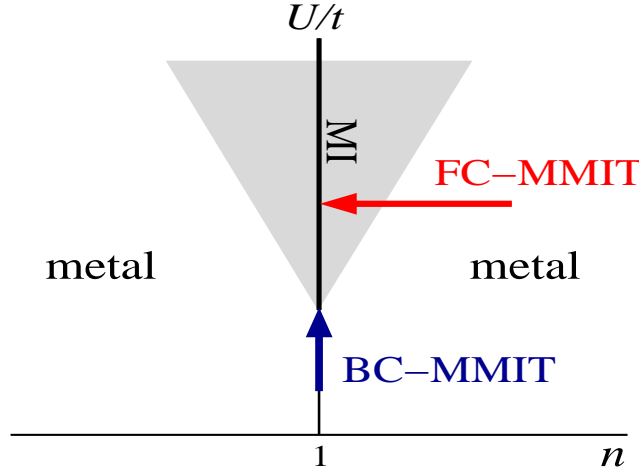

Fig. 1. General schematic phase diagram for the metal–Mott-insulator transition obtained from the Hubbard model. The shaded area represents a metallic region that is under the strong influence of the MMIT. The routes for the MMIT (see text) has been signaled with arrows.

It is well known that the Hubbard model [Eq. (1)] displays MMIT phase transitions at half filling and at finite values of the on-site repulsive interaction U [20]. (In the case of perfect nesting[1] the transition occurs at $U = 0$.) The schematic phase diagram is shown in Fig. 1, in the plane U/t vs n. The two routes for the MMIT are the filling-controlled MMIT (FC-MMIT), and the bandwidth-controlled MMIT (BC-MMIT) [20]. Metallic regions very close to the Mott-insulating phase [shaded area in Fig. 1] are under the strong

---

[1] Nesting refers to the existence of parallel sections in the Fermi surface. This means that excitations of vanishing energy are possible at finite momentum. Perfect nesting appears for periodic systems in 1D at any filling since in 1D the Fermi surface consists only of two points. In addition, it appears for hypercubic lattices at half filling since in those cases the Fermi surface is a hypercube.

influence of the MMIT, and in general exhibit anomalous features like mass enhancement and carrier number reduction [20]. In 1D systems, the metallic phase (Luttinger liquid) is characterized by gapless excitations and by a $2k_F$ (where k_F is the Fermi momentum) modulation of the spin-spin correlations. On the other side, in the Mott-insulating phase ($n = 1$) the system exhibits a charge gap, and quasi-long range antiferromagnetic correlations. At $n = 0, 2$ the system is in a trivial band insulating state.

3   The Hubbard model in a harmonic trap

Ultracold fermionic atoms on optical lattices represent nowadays the most direct experimental realization of the Hubbard model, since atoms interact only via a contact potential. In addition, in the experiments all parameters can be controlled with an unprecedented precision. Since the particles are trapped by a confined potential, it is possible to drive the MMIT by changing the total filling of the trap, the on-site repulsive interaction, or varying the curvature of the confining potential. The Hamiltonian in this case can be written as

$$H = -t \sum_{i,\sigma} \left(c_{i\sigma}^{\dagger} c_{i+1\sigma} + \text{H.c.} \right) + U \sum_{i} n_{i\uparrow} n_{i\downarrow} + V_2 \sum_{i\sigma} x_i^2 \ n_{i\sigma}, \qquad (2)$$

where V_2 is the curvature of the harmonic confining potential, and x_i measures the position of the site i ($x_i = ia$ with a the lattice constant). The number of lattice sites is N, and is selected so that all the fermions are confined in the trap. We denote the total number of fermions as N_f and consider equal number of fermions with spins up and down ($N_{f\uparrow} = N_{f\downarrow} = N_f/2$). In our simulations, we used the zero-temperature projector QMC method described in detail in Refs. [21,22,23].

Results for the evolution of the local density ($n_i = \langle n_{i\uparrow} + n_{i\downarrow} \rangle$), as a function of the total number of the confined particles, are shown in Fig. 2. For the lowest fillings, so that $n < 1$ at every site, the density shows a profile with the shape of an inverted parabola, similar to that obtained in the non-interacting case [24], and hence, such a situation should correspond to a metallic phase. Increasing the number of fermions a plateau with $n = 1$ appears in the middle of the trap, surrounded by a region with $n < 1$ (metallic). Since in the periodic case, a Mott insulator appears at $n = 1$, it is natural to identify the plateau with such a phase. The Mott-insulating domain in the center of the trap increases its size when more particles are added, but at a certain filling this becomes energetically unfavorable and a new metallic phase with $n > 1$ starts to develop in the center of the system. Upon adding more fermions, this new metallic phase widens spatially and the Mott-insulating domains surrounding it are pushed to the borders. Depending on the on-site repulsion strength, they can disappear and a complete metallic phase can appear in the system.
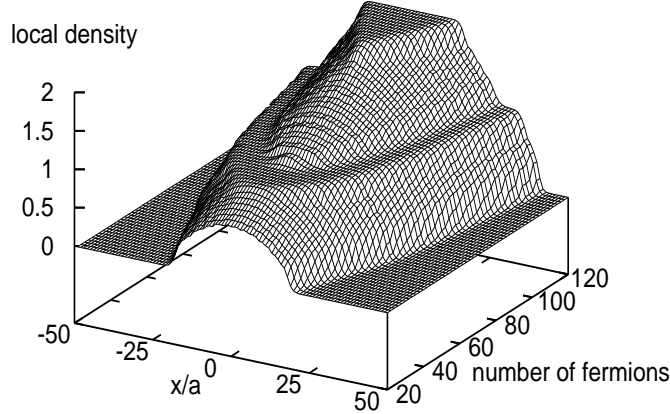
Fig. 2. Evolution of the local density in a parabolic confining potential as a function of the position in the trap and increasing total number of fermions. The parameters involved are $N = 100$, $U = 6t$ and $V_2a^2 = 0.006t$. The positions are measured in units of the lattice constant a.

Finally, a "band insulator" (i.e., $n = 2$) forms in the middle of the trap for the highest fillings. Due to the full occupancy of the sites, it will widen spatially and pushes the other phases present in the system to the edges of the trap when more fermions are added.

Alternatively to the case shown in Fig. 2, where the transitions between the phases were driven by an increment of the filling in the trap, Mott-insulating regions can be obtained by increasing the ratio U/t. Fig. 3(a) shows the evolution of the density profiles in a trapped system when this ratio is increased from $U/t = 2$ to $U/t = 8$. It can be seen that for small values of U/t ($U/t = 2$) there is only a metallic phase present in the trap. As the value of U/t ($U/t = 4$) is increased, a Mott-insulating phase tries to develop at $n = 1$ while a metallic phase with $n > 1$ is present in the center of the system. As the on-site repulsion is increased even further ($U/t = 6,\ 8$), a Mott-insulating domain appears in the middle of the trap suppressing the metallic phase that was present there. In Fig. 3(b) we show the variance of the density for the profiles in Fig. 3(a) (from top to bottom, the values presented are for $U/t = 2,\ 4,\ 6,\ 8$). As expected, the variance decreases in both the metallic and Mott-insulating phases when the on-site repulsion is increased. When the Mott-insulating plateau is formed in the density profile, a plateau with constant variance appears in the variance profile with a value that will vanish only in the limit $U/t \to \infty$. The dependence of the variance in the Mott insulator vs U/t is depicted in Fig. 3(d) up to $U/t = 20$ (five times the band-width). In this figure it is possible to see that after a fast decrease up to around $U/t = 8$, the variance reduces slowly [proportionally to $(U/t)^{-2}$] when increasing U. As shown in Fig. 3(b), whenever a Mott-insulating domain is formed in the trap, the value of the variance on it is exactly the same as the one for the Mott-insulating phase in the periodic system for the same value of U/t (horizontal dashed lines). This would support the validity of the commonly used local density (Thomas-

Fermi) approximation [25]. However, the insets in Fig. 3(b), show that this is not necessarily the case, since for $U/t = 4$, the value of the variance in the Mott-insulating phase of the periodic system is still not reached in the trap, although the density reaches the value $n = 1$. Therefore, in contrast to the periodic case, a Mott-insulating region is not only determined by the filling. In the cases of $U/t = 6$ [inset in Fig. 3(b) for a closer look] and $U/t = 8$, the value of the variance in the periodic system is reached and then one can say that Mott-insulating phases are formed there.
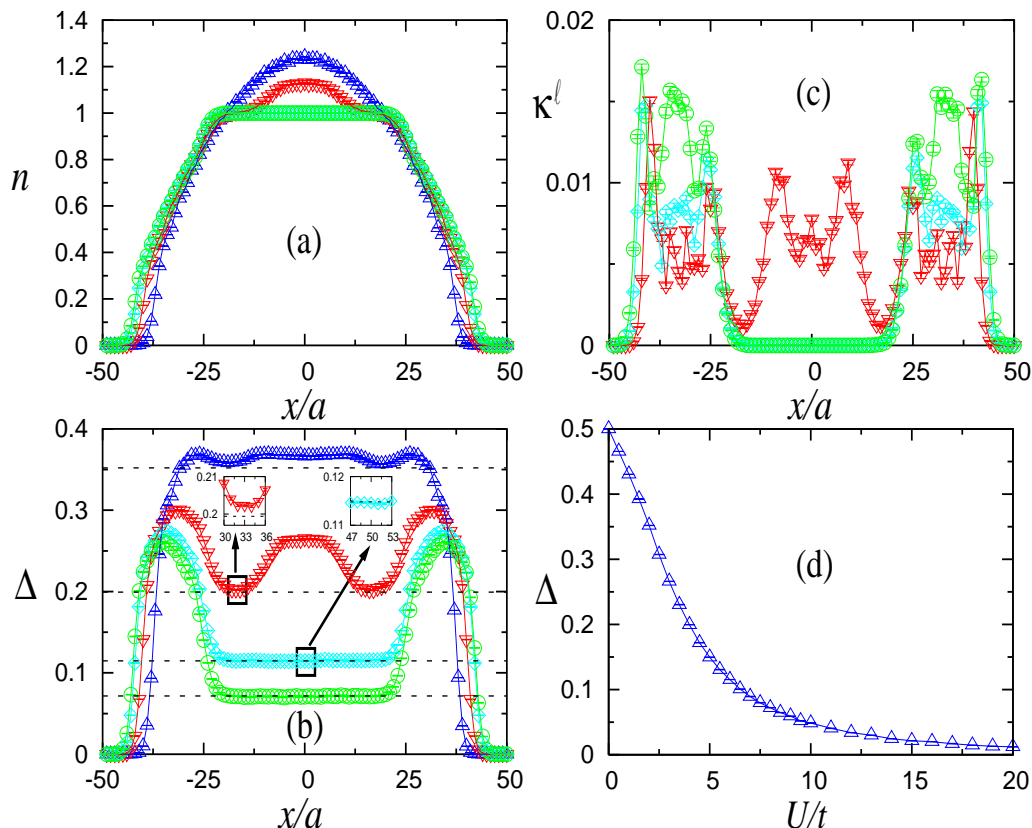

Fig. 3. Profiles for a trap with $V_2 a^2 = 0.0025t$ and $N_f = 70$, the on-site repulsions are U/t =2 ($\triangle$), 4 ($\triangledown$), 6 ($\diamond$), and 8 ($\bigcirc$). (a) Local density, (b) variance of the local density, (c) local compressibility κ^ℓ as defined in Eq. (3), (d) variance of the density in the Mott-insulating state (when $U/t > 0$) vs U/t. The dashed lines in (b) are the values of the variance in the $n = 1$ periodic system for $U/t = 2,\ 4,\ 6,\ 8$ (from top to bottom).

Although the variance gives a first indication for the formation of a local Mott insulator, an ambiguity is still present, since there are metallic regions with densities very close to $n = 0$ and $n = 2$, where the variance can have even smaller values than in the Mott-insulating phases. Therefore, an unambiguous quantity is still needed to characterize the Mott-insulating regions. We proposed a new local compressibility as a local-order parameter to characterize

the Mott-insulating regions[14,15], that is defined as

$$\kappa_i^\ell = \sum_{|j| \leq \ell(U)} \chi_{i,i+j} \; , \tag{3}$$

where

$$\chi_{i,j} = \langle n_i n_j \rangle - \langle n_i \rangle \langle n_j \rangle \tag{4}$$

is the density-density correlation function and $\ell(U) \simeq b\,\xi(U)$, with $\xi(U)$ the correlation length of $\chi_{i,j}$ in the unconfined system at half-filling for the given value of U. As a consequence of the charge gap opened in the Mott-insulating phase at half filling in the periodic system, the density-density correlations decay exponentially $[\chi_{(x)} \propto \exp^{-\frac{x}{\xi(U)}}]$ enabling $\xi(U)$ to be determined. The factor b is chosen within a range where κ^ℓ becomes qualitatively insensitive to its precise value ($b \sim 10$) [15]. Physically, the local compressibility defined here gives a measure of the change in the local density due to a constant shift of the potential over a finite range but over distances larger than the correlation length in the unconfined system.

In Fig. 3(c), we show the profiles of the local compressibility for the same parameters as Figs. 3(a) and (b) (we did not include the profile of the local compressibility for $U = 2t$ because for that value of U we obtain that ℓ is bigger than the system size). In Fig. 3(c), it can be seen that the local compressibility only vanishes in the Mott-insulating domains. For $U = 4t$, it can be seen that in the region with $n \sim 1$ the local compressibility, although small, does not vanish. This is compatible with the fact that the variance is not equal to the value in the periodic system there, so that although there is a shoulder in the density profile, this region is not a Mott insulator. Therefore, the local compressibility defined here serves as a genuine local order parameter to characterize the insulating regions that always coexist with metallic phases.

4   Local quantum criticality and universality

In the previous section we have characterized the local Mott-insulating and metallic phases quantitatively. We study in this section the regions where the system goes from one phase to another. Criticality can arise, despite the microscopic spatial size of the transition region [2], due to the extension in imaginary time that reaches the thermodynamic limit at $T = 0$, very much like the case of the single impurity Kondo problem [26], where long-range interactions in imaginary time appear for the local degree of freedom as a result of the interaction with the rest of the system. An intriguing future question, for

---

[2] Recent experiments leading to a MMIT [8,9] considered a systems with linear dimensions $\sim 100a$, i.e. still in a microscopic range.

both theory and experiment, will be the role of spatial dimension in the critical behavior of systems in the thermodynamic limit. In the periodic case, the FC-MMIT in 1D and 2D belong to different universality classes, with dynamical exponents $z = 2$ (1D) and $z = 4$ (2D) [20]. This route to the transition in the periodic case, is the one relevant for the trapped systems where the density changes on entering in the local Mott insulator, and could lead to different local quantum critical behavior between traps with different dimensionalities. In the bosonic case the FC-MMIT exhibits the same dynamical exponent ($z = 2$) in all dimensions [27,28], which could also lead to a different local quantum critical behavior for trapped bosons as compared with trapped fermions.
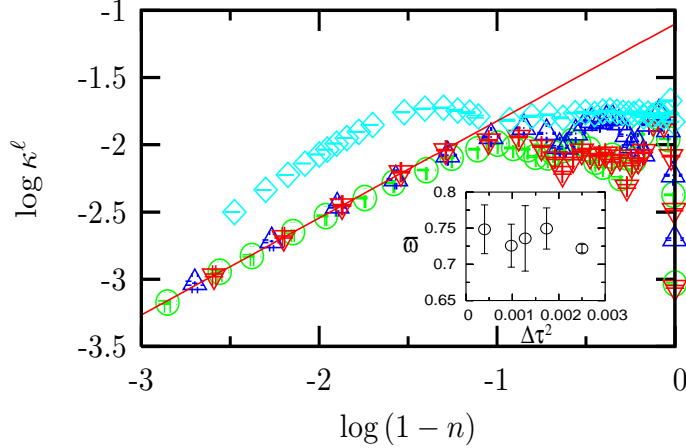

Fig. 4. The local compressibility κ^ℓ vs $\delta = 1 - n$ at $\delta \to 0$ for ($\triangle$) $N_f = 70$, $U = 8t$ and $V_2 a^2 = 0.0025t$; ($\triangledown$) $N_f = 70$, $U = 6t$ and $V_2 a^2 = 0.0025t$; ($\bigcirc$) $N_f = 72$, $U = 6t$ and a quartic potential with $V_4 a^4 = 1.0 \times 10^{-6}t$; ($\diamond$) unconfined periodic system with $U = 6t$. The straight line displays a power-law behavior $\varpi = 0.72$. Inset: Dependence of the critical exponent ϖ on $\Delta\tau^2$.

Figure 4 shows the local compressibility vs $\delta = 1 - n$ for $\delta \to 0$ in a double logarithmic plot. A power law $\kappa^\ell \sim \delta^\varpi$ is obtained, with $\varpi < 1$, such that a divergence results in its derivative with respect to n, showing that critical fluctuations are present in this region. Since the QMC simulation is affected by systematic errors due to discretization in imaginary time, it is important to consider the limit $\Delta\tau \to 0$ in determining the critical exponent. The inset in Fig. 4 shows such an extrapolation leading to $\varpi \simeq 0.68 - 0.78$. At this point we should remark that the presence of the harmonic potential allows the determination of the density dependence of various quantities with unprecedented detail on feasible system sizes as opposed to unconfined periodic systems, where systems with $10^3 - 10^4$ sites would be necessary to allow for similar variations in density. In addition to the power law behavior, Fig. 4 shows that for $\delta \to 0$, the local compressibility of systems with a harmonic potential but different strengths of the interaction or even with a quartic confining potential, collapse on the same curve. Hence, universal behavior as expected for critical phenomena is observed also in this case. This fact is particularly important with regard to experiments, since it implies that the observation of criticality

8

should be possible for realistic confining potentials, and not only restricted to perfect harmonic ones, as usually used in theoretical calculations. However, Fig. 4 shows also that the unconfined case departs from all the others. Up to the largest systems we simulated (600 sites), we observe an increasing slope rather than the power law of the confined systems. Actually, we observe that the exponent of the power law obtained between contiguous points in Fig. 4 for the periodic case extrapolates to $\varpi = 1$, as it is shown in Fig. 5.
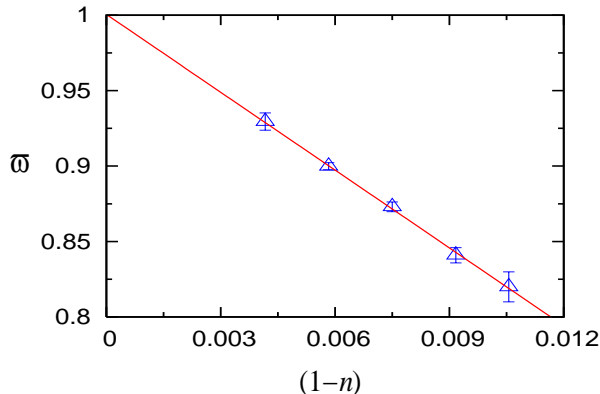
Fig. 5. Exponent ϖ of the local compressibility for the periodic system, obtained between contiguous points in Fig. 4, vs $(1-n)$. The extrapolation leads to $\varpi = 1$ for $n \to 1$.

Having shown that the local compressibility displays universality on approaching a Mott-insulating region, we consider the variance Δ as a function of the density n for various values of U and different confining potentials. Figure 6 shows Δ vs n for a variety of systems, where not only the number of particles and the size of the system are changed, but also different forms of the confining potential were used. Here we considered a harmonic potential, a quartic one, and a superposition of a harmonic, a cubic and a quartic one, such that even reflection symmetry across the center of the system is broken. It appears at first glance that the data can only be distinguished by the strength of the interaction U, showing that the variance is rather insensitive to the form of the potential. The different insets, however, show that a close examination leads to the conclusion that only near $n = 1$ and only in the situations where at $n = 1$ a Mott insulator exists, universality sets in. The inset for n around 0.6 and $U = 8t$, shows that the unconfined system has different variance from the others albeit very close on a raw scale. This difference is well beyond the error bars. Also the inset around $n = 1$ and for $U = 4t$, shows that systems that do not form a Mott-insulating phase in spite of reaching a density $n = 1$, have a different variance from those having a Mott insulator. Only the case where all systems have a Mott-insulating phase at $n = 1$ ($U = 8t$), shows universal behavior independent of the potential, a universality that encompasses also the unconfined systems. For the unconfined system, the behavior of the variance can be examined with Bethe-*Ansatz* [29] in the limit $\delta \to 0$.
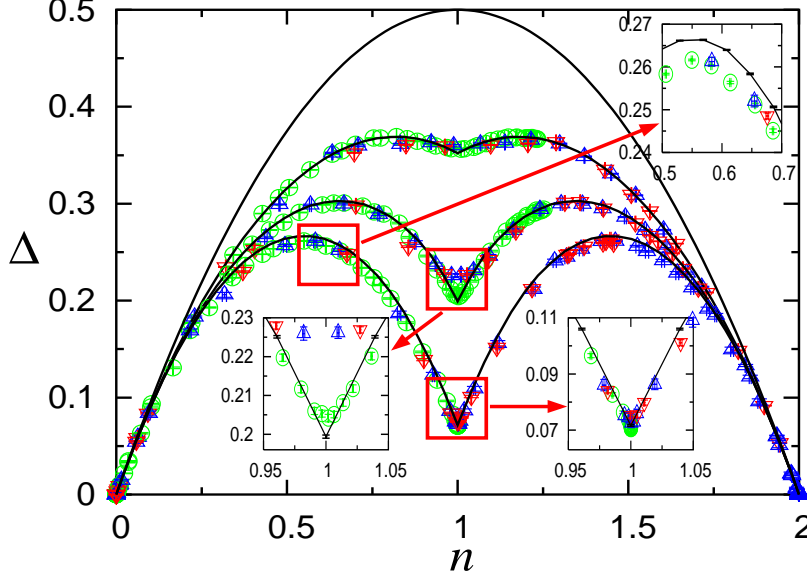
9

Fig. 6. Variance Δ *vs.* n for ($\bigcirc$) harmonic potential $V_2 a^2 = 0.0025t$ with $N = 100$; ($\triangle$) quartic potential $V_4 a^4 = 5 \times 10^{-7} t$ with $N = 150$; ($\triangledown$) harmonic potential $V_2 a^2 = 0.016t$ + cubic $V_3 a^3 = 1.6 \times 10^{-4} t$ + quartic $V_4 a^4 = 1.92 \times 10^{-5} t$ with $N = 50$; and (full line) unconfined periodic potential with $N = 102$ sites. The curves correspond from top to bottom to $U/t = 0, 2, 4, 8$. For a discussion of the insets, see text.

In this limit and to leading order in δ, the ground state energy is given by [30] $E_0(\delta)/N - E_0(\delta = 0)/N \propto \delta$, such that the double occupancy, which can be obtained as the derivative of the ground-state energy with respect to U, will also converge as δ towards its value at half-filling. Such behavior is also obtained in our case as shown in Fig. 7 for the same parameters of Fig. 4.
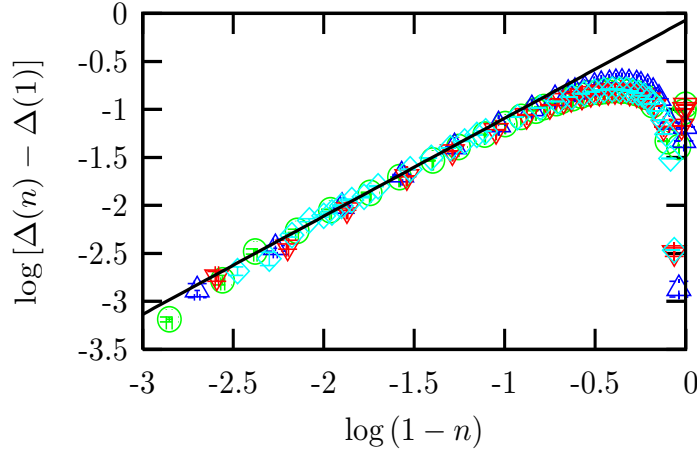

Fig. 7. Variance of the density vs $\delta = 1 - n$ at $\delta \to 0$ for ($\triangle$) $N_f = 70$, $U = 8t$ and $V_2 a^2 = 0.0025t$; ($\triangledown$) $N_f = 70$, $U = 6t$ and $V_2 a^2 = 0.0025t$; ($\bigcirc$) $N_f = 72$, $U = 6t$ and a quartic potential with $V_4 a^4 = 1.0 \times 10^{-6} t$; ($\diamond$) unconfined periodic system with $U = 6t$. The straight line displays linear behavior, i.e. its slope is equal to one.

5 Momentum distribution function

In most experiments with quantum gases carried out so far, the MDF, which is determined in time-of-flight measurements, played a central role. A prominent example is given by the study of the superfluid–Mott-insulator transition [8] in the bosonic case. As shown below, we find that the MDF is not appropriate to characterize the phases of the system in the fermionic case, and does not show any clear signature of the MMIT.
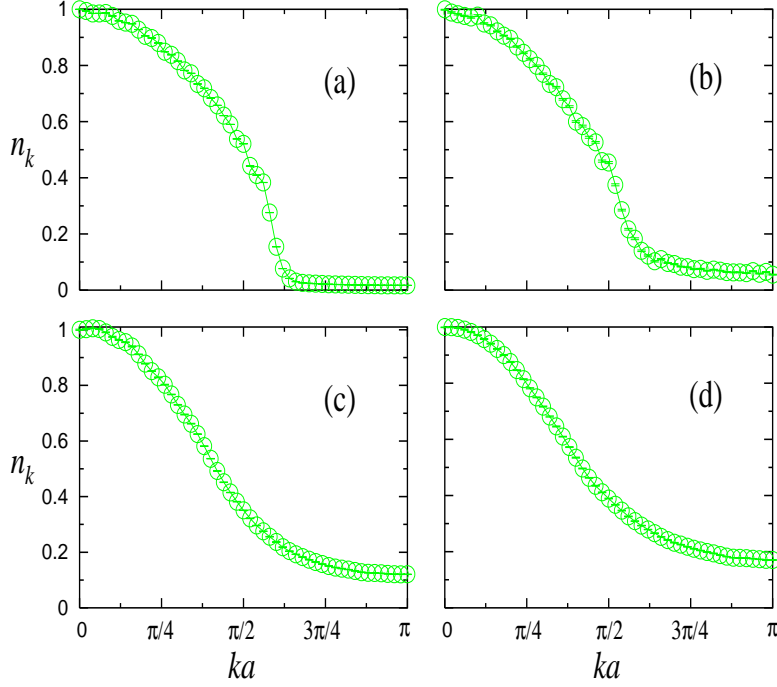

Fig. 8. Normalized momentum distribution function for $U/t = 2$ (a) 4 (b), 6 (c), 8 (d), and $N = 100$, $N_f = 70$, $V_2 a^2 = 0.0025t$.

In Fig. 8 we show the normalized momentum distribution function for the density profiles shown in Fig. 3. For the trapped systems, we always normalize the MDF to be unity at $k = 0$. We first notice that n_k for the pure metallic phase in the harmonic trap [Fig. 8(a)] does not display any sharp feature corresponding to a Fermi surface, in clear contrast to the periodic case. The lack of a sharp feature for the Fermi surface is independent of the presence of the interaction and is also independent of the size of the system. In the non-interacting case, this can be easily understood: the spatial density and the momentum distribution will have the same functional form because the Hamiltonian is quadratic in both coordinate and momentum. When the interaction is present, it could be expected that the formation of local Mott-insulating domains generates a qualitatively and quantitatively different behavior of the momentum distribution, like in the periodic case where in the Mott-insulating phase the Fermi surface disappears. In Fig. 8(c), it can be seen that there is

no qualitative change of the MDF when the Mott-insulating phase is present in the middle of the trap. Quantitatively n_k in this case is similar to the pure metallic cases Fig. 8(a),(b). Quantitative changes in n_k appear only when the on-site repulsion goes to the strong-coupling regime, but this is long after the Mott-insulating phase has appeared in the system.

At this point one might think that in order to study the MMIT using the MDF, it is necessary to avoid the inhomogeneous trapping potential and use instead a kind of magnetic box with infinitely high potential on the boundaries. However, in that case one of the most important achievements of the inhomogeneous system is lost, i.e., the possibility of creating Mott-insulating phases for a continuous range of fillings. In the perfect magnetic box, the Mott-insulating phase would only be possible at half filling, which would be extremely difficult (if possible at all) to adjust experimentally. The other possibility is to create traps which are almost homogenous in the middle and which have an appreciable trapping potential only close to the boundaries. This can be studied theoretically by considering traps with higher powers of the trapping potentials. As shown below, already non-interacting systems make clear that a sharp Fermi edge is missing in confined systems.
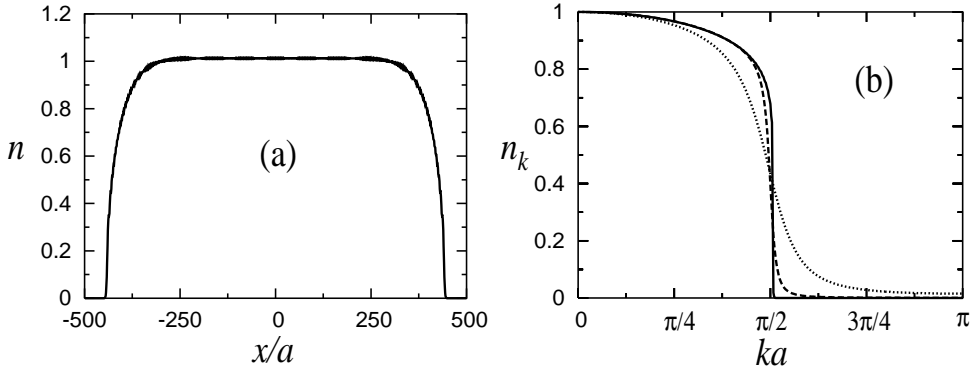

Fig. 9. Exact results for $N_f = 840$ noninteracting trapped fermions in a lattice with 1000 sites and a confining potential $V_{10}a^{10} = 7 \times 10^{-27}t$. Density profile (a) and the normalized momentum distribution function (b): the continuous line corresponds to (a), the dashed line is the result when an alternating potential $V_a = 0.1t$ is superposed on the system, and the dotted line corresponds to $V_a = 0.5t$.

In Fig. 9(a) we show the density profile of a system with 1000 sites, $N_f = 840$, and a trapping potential of the form $V_{10}x_i^{10}$ with $V_{10}a^{10} = 7 \times 10^{-27}t$. It can be seen that the density is almost flat all over the trap with a density of the order of one particle per site. Only a small part of the system at the borders has the variation of the density required for the particles to be trapped. In Fig. 9(b) (continuous line), we show the corresponding normalized momentum distribution. It can be seen that a kind of Fermi surface develops in the system but for smaller values of k, n_k is always smooth and its value starts decreasing at $k = 0$. In order to see how n_k changes when an incompressible region appears in the system, we introduced an additional alternating potential, so

12

that in this case the new Hamiltonian has the form

$$H = -t \sum_{i,\sigma}(c_{i\sigma}^{\dagger}c_{i+1\sigma} + \text{H.c.}) + V_{10}\sum_{i\sigma}x_i^{10}\,n_{i\sigma} + V_a\sum_{i\sigma}(-1)^i\,n_{i\sigma}, \qquad (5)$$

where V_a is the strength of the alternating potential. For the parameters presented in Fig. 9(a), we obtain that a small value of V_a ($V_a = 0.1t$) generates a band insulator in the trap, which extends over the region with $n \sim 1$ (when $V_a = 0$). However, the formation of this band insulator is barely reflected in n_k, as can be seen in Fig. 9(b) (dashed line). Only when the value of V_a is increased and the system departs from the phase transition [$V_a = 0.5t$, dotted line in Fig. 9(c)], does a quantitatively appreciable change in n_k appear.

6   Phase Diagram

Finally we consider the phase diagram of the system. As shown in Figs. 2 and 3, unlike the exponents, phase boundaries seem to be rather sensitive to the choice of potential, number of particles and strength of the interaction. As in the unconfined case, we would expect to be able to relate systems with different number of particles and/or sizes by their density. Given the harmonic potential, a characteristic length (in units of the lattice constant) is given by $\zeta = (V_2/t)^{-1/2}$, such that a characteristic density can be defined. Figure 10 shows that the characteristic density $\tilde{\rho} = N_f/\zeta$ is a meaningful quantity to characterize the phase diagram. There, the phase diagrams for two systems
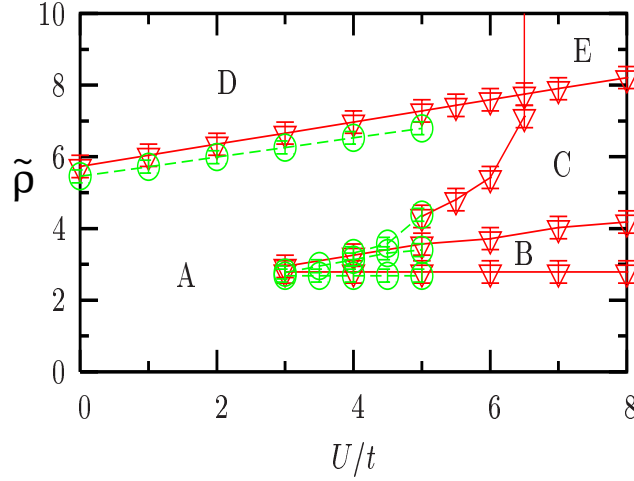

Fig. 10. Phase diagram for a system with $N = 100$, $V_2a^2 = 0.006t$ ($\triangledown$) and $N = 150$, $V_2a^2 = 0.002t$ ($\bigcirc$) sites. The phases are explained in the text.

with different sizes ($N = 100$ and $N = 150$) and different strength of the harmonic potential ($V_2a^2 = 0.006t$ and $V_2a^2 = 0.002t$ respectively) are depicted

13

showing that such a scaling allows to compare systems with different sizes, different number of particles, and different strength of the potential. With this, it is possible to relate the results of numerical simulations to much larger experimental systems. The different phases obtained are: A pure metal without insulating regions (A), a Mott-insulator at the center of the trap (B), a metallic intrusion at the center of a Mott-insulator (C), a "band insulator" (i.e. with $n = 2$) at the center of the trap surrounded by a metal (D), and finally a "band insulator" surrounded by a metal, surrounded by a Mott-insulator with the outermost region being again a metal (E). Two features are remarkable here. The first one is that on varying the filling of the trap, a reentrant behavior is observed for the phase A. The density profile shows a shoulder as can be seen in Fig. 2 before reaching the plateau with $n = 2$ but, as shown by the inset of Fig. 3 for $U = 4$ around $n = 1$, it is possible to go through a region with $n = 1$ without reaching the value of the variance that corresponds to a Mott-insulator. The second intriguing feature is that the boundary between the regions A and B remains at the same value of the characteristic density for all values of U that could be simulated. The latter feature is consistent with the fact that for $U \to \infty$ density properties of two-component fermionic systems become identical to the ones of single species fermions with the same total filling. In this case, the characteristic density for the formation of the insulating state with $n = 1$ in the middle of the trap was obtained in Ref. [31] $\tilde{\rho} \sim 2.6 - 2.7$. This is the same value observed in Fig. 10 for the formation of the Mott insulator. A comparison between density profiles for systems with a Mott insulator in the middle of the trap for $U/t = 8$ and $U/t = \infty$ is presented in Fig. 11(a). No big differences are observed between both cases. This is clearly in contrast to the comparison of the variance profiles [Fig. 11(b)] where in the Mott plateau the variance has changed abruptly.
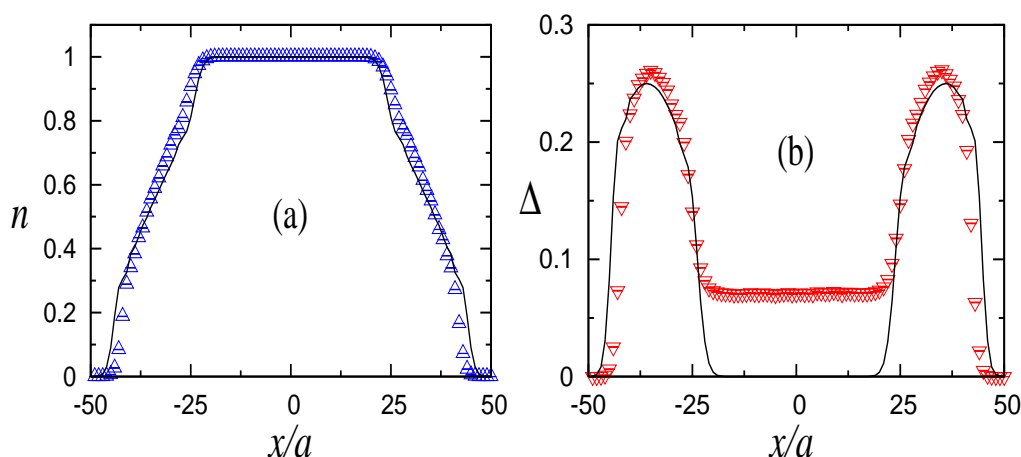

Fig. 11. Comparison between density ($\triangle$) and variance ($\triangledown$) profiles for a system with $U/t = 8$ and a system with $U/t = \infty$ (continuous line). In both cases $V_2 a^2 = 0.0025t$ and $N_f = 70$.

14

7 Conclusions

We have studied ground state properties of two-species fermions confined on 1D optical lattices, reviewing and enhancing the analysis in Refs. [14,15]. We have defined a local-order parameter, that we called local compressibility, which characterizes the local insulating regions in an unambiguous way. It vanishes in the insulating phases and is finite in the metallic ones. This local compressibility gives a measure of the local change in density due to a constant shift of the potential over finite distances larger than the correlation length of the density-density correlation function for the Mott-insulating phase in the unconfined system. We found that the local compressibility exhibits critical behavior (a power-law decay $\kappa^l \sim |1 - n|^\varpi$) on entering the Mott-insulating regions. Due to the microscopic nature of the phases, spatial correlations appear not to contribute to the critical behavior discussed there. This is a new form of metal–Mott-insulator transition not observed so far in simple periodic systems, and that might be realized in fermionic gases trapped on optical lattices. The exponent of the power-law (ϖ) was obtained to be independent of the confining potential and/or strength of the interaction, excluding, however, the unconfined case. Universal behavior was also observed for the variance $\Delta \sim |1 - n|$ when $n \to 1$. In this case, the observed behavior is shared by the unconfined model.

As opposed to periodic systems, where the appearance of the gap in the insulating phase can be seen by the disappearance of the Fermi surface in the momentum distribution function, we found that due to the presence of a harmonic confining potential such a feature is much less evident. In a non-interacting case, we have shown that although increasing the power of the confining potential sharpens the features connected with the Fermi edge, it remains qualitatively different from the homogeneous case. Hence, in fermionic systems the momentum distribution function does not seem to be the appropriate quantity to detect experimentally the formation of Mott-insulating domains.

Finally, we determined a generic form for the phase diagram that allows to compare systems with different values of all the parameters involved in the model. It can be used to predict the phases that will be present in future experimental results. The phase diagram also reveals interesting features such as reentrant behavior in some phases when parameters are changed, and phase boundaries with linear forms. Results obtained for finite values of the on-site repulsion were contrasted with the ones for infinite U. We observe that once a Mott plateau has appeared in the middle of the trap, density profiles do not change much by increasing the on-site repulsion. This is in contrast to the variance of the density, which reduces continuously to zero in the Mott-insulating phase.

Acknowledgments

References

[1] F. Dalfovo, S. Giorgini, L. P. Pitaevskii, and S. Stringari, Rev. Mod. Phys. **71**, 463 (1999).

[2] A. J. Leggett, Rev. Mod. Phys. **73**, 307 (2001).

[3] C. J. Pethick and H. Smith, *Bose-Einstein Condensation in Dilute Gases* (Cambridge University Press, Cambridge, 2002).

[4] L. P. Pitaevskii and S. Stringari, *Bose-Einstein Condensation* (Oxford University Press, Oxford, 2003).

[5] M. H. Anderson, J. R. Ensher, M. R. Matthews, C. E. Wieman, and E. A. Cornell, Science **269**, 198 (1995).

[6] C. C. Bradley, C. A. Sackett, J. J. Tollett, and R. G. Hulet, Phys. Rev. Lett. **75**, 1687 (1995).

[7] K. B. Davis, M.-O. Mewes, M. R. Andrews, N. J. van Druten, D. S. Durfee, D. M. Kurn, and W. Ketterle, Phys. Rev. Lett. **75**, 3969 (1995).

[8] M. Greiner, O. Mandel, T. Esslinger, T. W. Hänsch, and I. Bloch, Nature **415**, 39 (2002).

[9] T. Stöferle, H. Moritz, C. Schori, M. Köhl, and T. Esslinger, Phys. Rev. Lett. **92**, 130403 (2004).

[10] D. Jaksch, C. Bruder, J. I. Cirac, C. W. Gardiner, and P. Zoller, Phys. Rev. Lett. **81**, 3108 (1998).

[11] G. G. Batrouni, V. Rousseau, R. T. Scalettar, M. Rigol, A. Muramatsu, P. J. H. Denteneer, and M. Troyer, Phys. Rev. Lett. **89**, 117203 (2002).

[12] V. A. Kashurnikov, N. V. Prokof'ev, and B. V. Svistunov, Phys. Rev. A **66**, 031601(R) (2002).

[13] S. Wessel, F. Alet, M. Troyer, and G. G. Batrouni, cond-mat/0404552.

[14] M. Rigol, A. Muramatsu, G. G. Batrouni, and R. T. Scalettar, Phys. Rev. Lett. **91**, 130403 (2003).

[15] M. Rigol and A. Muramatsu, Phys. Rev. A **69**, 053612 (2004).

[16] G. Modugno, F. Ferlaino, R. Heidemann, G. Roati, and M. Inguscio, Phys. Rev. A **68**, 011601(R) (2003).

[17] H. Ott, E. de Mirandes, F. Ferlaino, G. Roati, G. Modugno, and M. Inguscio, Phys. Rev. Lett. **92**, 160601 (2004).

[18] P. W. Anderson, Phys. Rev. **115**, 2 (1959).

[19] J. Hubbard, Proc. R. Soc. London A **276**, 238 (1963).

[20] M. Imada, A. Fujimori, and Y. Tokura, Rev. Mod. Phys. **70**, 1039 (1998).

[21] E. Y. Loh and J. E. Gubernatis, in *Modern Problems in Condensed Matter Sciences*, edited by W. Hanke and Y. V. Kopaev (North-Holland, Amsterdam, 1992), Vol. 32, pp. 177–235.

[22] A. Muramatsu, in *Quantum Monte Carlo Methods in Physics and Chemistry*, edited by M. P. Nightingale and C. J. Umrigar (NATO Science Series, Kluwer Academic Press, Dordrecht, 1999), pp. 343–373.

[23] F. F. Assaad, in *Quantum Simulations of Complex Many-Body Systems: From Theory to Algorithms*, edited by J. Grotendorst, D. Marx, and A. Muramatsu (John von Neumann Institute for Computing (NIC) Series, Vol. 10, FZ-Jülich, 2002), pp. 99–155.

[24] P. Vignolo, A. Minguzzi, and M. P. Tosi, Phys. Rev. Lett. **85**, 2850 (2000).

[25] D. A. Butts and D. S. Rokhsar, Phys. Rev. A **55**, 4346 (1997).

[26] G. Yuval and P. Anderson, Phys. Rev. B **1**, 1522 (1970).

[27] M. P. A. Fisher, P. B. Weichman, G. Grinstein, and D. S. Fisher, Phys. Rev. B **40**, 546 (1989).

[28] G. G. Batrouni, R. T. Scalettar, and G. T. Zimanyi, Phys. Rev. Lett. **65**, 1765 (1990).

[29] E. H. Lieb and F. Y. Wu, Phys. Rev. Lett. **20**, 1445 (1968).

[30] A. Schadschneider and J. Zittartz, Z. Phys. B **82**, 387 (1991).

[31] M. Rigol and A. Muramatsu, Phys. Rev. A **70**, 043627 (2004).

[32] B. A. Berg, Comp. Phys. Commun. **69**, 7 (1992).